



HAL
open science

New Class of Laboratory Astrophysics Experiments: Application to Radiative Accretion Processes around Neutron Stars

V. Tranchant, N. Charpentier, L. van Box Som, A. Ciardi, É. Falize

► **To cite this version:**

V. Tranchant, N. Charpentier, L. van Box Som, A. Ciardi, É. Falize. New Class of Laboratory Astrophysics Experiments: Application to Radiative Accretion Processes around Neutron Stars. *The Astrophysical Journal*, 2022, 936, 10.3847/1538-4357/ac81b8 . insu-03851609

HAL Id: insu-03851609

<https://insu.hal.science/insu-03851609>

Submitted on 14 Nov 2022

HAL is a multi-disciplinary open access archive for the deposit and dissemination of scientific research documents, whether they are published or not. The documents may come from teaching and research institutions in France or abroad, or from public or private research centers.

L'archive ouverte pluridisciplinaire **HAL**, est destinée au dépôt et à la diffusion de documents scientifiques de niveau recherche, publiés ou non, émanant des établissements d'enseignement et de recherche français ou étrangers, des laboratoires publics ou privés.



Distributed under a Creative Commons Attribution 4.0 International License



New Class of Laboratory Astrophysics Experiments: Application to Radiative Accretion Processes around Neutron Stars

V. Tranchant^{1,2} , N. Charpentier¹, L. Van Box Som^{1,3}, A. Ciardi², and É. Falize¹

¹CEA, DAM, DIF, F-91297 Arpajon, France; victor.tranchant@obspm.fr

²LERMA, Sorbonne Université, Observatoire de Paris, Université PSL, CNRS, F-75005, Paris, France

³Université Paris-Saclay, CEA, LMCE, F-91680 Bruyères-le-Châtel, France

Received 2022 April 20; revised 2022 July 14; accepted 2022 July 16; published 2022 August 25

Abstract

Extreme radiative phenomena, where the radiation energy density and flux strongly influence the medium, are common in the universe. Nevertheless, because of limited or nonexistent observational and experimental data, the validity of theoretical and numerical models for some of these radiation-dominated regimes remains to be assessed. Here, we present the theoretical framework of a new class of laboratory astrophysics experiments that can take advantage of existing high-power laser facilities to study supersonic radiation-dominated waves. Based on an extension of Lie symmetry theory we show that the stringent constraints imposed on the experiments by current scaling theories can in fact be relaxed, and that astrophysical phenomena can be studied in the laboratory even if the ratio of radiation energy density to thermal energy and systems' microphysics are different. The validity of this approach holds until the hydrodynamic response of the studied system starts to play a role. These equivalence symmetries concepts are demonstrated using a combination of simulations for conditions relevant to Type I X-ray burst and of equivalent laboratory experiments. These results constitute the starting point of a new general approach expanding the catalog of astrophysical systems that can be studied in the laboratory.

Unified Astronomy Thesaurus concepts: Neutron stars (1108); Accretion (14); Scaling relations (2031); Laboratory astrophysics (2004); X-ray sources (1822)

1. Introduction

Extreme radiation-dominated phenomena abound in the universe and are often associated with accretion of matter in compact objects, and the subsequent release of intense radiation into the surrounding environment. One example is the sudden thermonuclear explosion of the envelope of a neutron star as it accretes matter from a companion star via an accretion disk. These so-called Type I X-ray bursts (XRBs) generate (Lewin et al. 1993; Galloway & Keek 2021) an intense X-ray radiation with a luminosity $\sim 10^{38}$ erg.s⁻¹ that is generally characterized by a fast rise time, ~ 1 s, followed by a slower exponential or power-law decay ~ 10 s (Lewin et al. 1993). These recurrent radiation bursts are believed to strongly affect the inner regions of the accretion disk (Ballantyne & Everett 2005).

In general, an intense burst of radiation can drive in the surrounding environment a heat front that propagates at supersonic speeds. Recently, this type of radiatively driven wave was observed as a subluminal thermal radiation heat wave propagating from a high-mass protostar during an accretion burst event (Burns et al. 2020). Radiatively driven waves also play a key role in preshock heating of matter in the early solar nebula (Morris et al. 2016). Ionization fronts, such as those generated around massive stars by photoionizing radiation impinging on their molecular environment (Walch et al. 2012; Dale et al. 2014), are another example of radiatively driven waves, albeit heating in these cases is less important. In the laboratory, radiatively driven supersonic heat waves (in short RWs) are known as Marshak waves (Marshak 1958; Hammer & Rosen 2003), and have been produced (Back et al. 2000a, 2000b; Moore et al. 2015) using

high-power lasers to generate a burst of X-rays radiation that irradiates and propagates in a low-density homogeneous medium. However, the radiative regimes achieved in the laboratory have so far been limited to relatively small radiative energy densities when compared to the thermal energy density.

To date, there are no detailed observational or experimental data of RWs in the radiation-dominated regime, which is relevant to many astrophysical systems. Furthermore, although numerical simulations continue to be the only means to study these phenomena, their validity remains to be assessed. The framework for scaling astrophysical phenomena to the laboratory (Ryutov et al. 1999; Falize et al. 2011a) has been the basis for many high-energy density plasma experiments, such as those studying physical processes relevant to accretion shocks (Falize et al. 2012; Krauland et al. 2012, 2013; Cross et al. 2016; Revet et al. 2017; Van Box Som et al. 2018; Mabey et al. 2019), magnetized stellar jets (Lebedev et al. 2005; Ciardi et al. 2007, 2009, 2013; Albertazzi et al. 2014; Revet et al. 2021), supernova remnants (Kuranz et al. 2018; Rigon et al. 2019; Albertazzi et al. 2020), or accretion disks (Valenzuela-Villaseca et al. 2022). However, these similarity concepts require experiments to reach the same physical regime as found in astrophysics, as well as to keep the microphysics of the two systems similar. For RWs in the radiation-dominated regime, these constraints mean that current high-power laser facilities are unable to produce them in the laboratory.

To go beyond the limitations imposed by similarity concepts, we develop in this article a new class of laboratory astrophysics experiments based on the resemblance concept (Takabe 2001). This purports to compare systems described by the same global physical models but potentially evolving in different physical regimes and governed by nonsimilar microphysical processes. We obtain explicit resemblance transformations by studying equivalence transformations (Ovsiannikov 1982; Olver 1986)



Original content from this work may be used under the terms of the [Creative Commons Attribution 4.0 licence](https://creativecommons.org/licenses/by/4.0/). Any further distribution of this work must maintain attribution to the author(s) and the title of the work, journal citation and DOI.

based on an extension of the Lie classical theory of symmetries of differential equations. We apply these newly found concepts to the case of RWs generated by Type I XRBs, and show that existing high-power laser facilities should be able to study them in the laboratory.

2. Interaction of X-Ray Bursts with Accretion Disks

We start here by showing that RWs should be present in accretion disks irradiated by Type I XRBs. Theoretical predictions of the effects of X-ray heating on the disk (Ballantyne & Everett 2005) were recently investigated through general relativistic, radiation hydrodynamics simulations (Fragile et al. 2018, 2020). These simulations have shown that over the burst timescale, and within the inner few hundreds of kilometers of the disk, the intense burst of X-ray radiation has a dramatic effect on the disk structure and temperature, highlighting, for example, an increase in the local accretion rate by a factor of $\sim 3\text{--}4$ due to the Poynting–Robertson drag effect.

To study RWs and the XRB-disk interaction, we build a simplified one-dimensional model of the inner regions of the accretion disk. For the temporal profile of the radiation source, we follow the approach of Fragile et al. (2020) who used a model developed by Norris et al. (2005) that matches typical XRB observational profiles. Considering the burst radiation spectrum to behave as a blackbody (Keek et al. 2018), the evolution of the radiation source is described in terms of temperature

$$T_{\text{XRB}}(t) = T_p \exp \left[\frac{1}{2} \sqrt{\frac{\tau_1}{\tau_2}} + \frac{1}{4} \frac{\tau_1}{t_0 - t} + \frac{1}{4} \frac{t_0 - t}{\tau_2} \right] \quad (1)$$

with T_p the peak temperature and t_0 , τ_1 , and τ_2 constant parameters shaping the burst. We take $T_p = 1$ keV and parameters $t_0 = -0.09$ s, $\tau_1 = 1$ s, $\tau_2 = 1.5$ s to obtain a typical burst shape with a rise timescale $t_{\text{rise}} \sim 1$ s.

The density and temperature of the inner region of the accretion disk are not well constrained by observations. For our simplified model, whose aim is to probe the basic features of the burst-disk interaction and the propagation of RWs, we neglect the disk's density gradients over length scales $L \leq \rho/|\nabla\rho|$ of a few hundred kilometers, and take the density of the disk, ρ_0 , to be constant. After exploring a wide range of densities, $10^{-1}\text{--}10^{-5}$ g cm $^{-3}$, consistent with theoretical predictions, we chose $\rho_0 = 10^{-4}$ g cm $^{-3}$ to isolate the propagation of RWs over characteristic times, $t \sim 10^{-2}$ s, shorter than any other predicted mechanisms (Ballantyne & Everett 2005). The initial temperature of the disk is initially taken to be uniform $T_0 = 50$ eV. We note that modifying the initial temperature value does not change the qualitative physical evolution of the RW, as it only affects slightly the radiative front velocity and structure. Finally, given the expected short timescale of propagation of the RWs ($\simeq 10^{-3}$ s) compared to the rotation of the disk, the latter can be neglected.

For the plasma conditions in the disk the opacity is dominated by elastic scattering on free electrons, as shown by comparing the photon energy and the electron rest energy:

$$\frac{h\nu}{m_e c^2} \simeq 2 \times 10^{-3} \ll 1 \quad (2)$$

with $h = 6.62 \times 10^{-27}$ erg.s the Planck constant, $\nu \simeq 2.4 \times 10^{17}$ Hz the photon frequency, $m_e = 9.11 \times 10^{-28}$ g the electron mass, and $c = 3 \times 10^{10}$ cm s $^{-1}$ the vacuum light speed. Then, the Rosseland opacity κ_R is expected to be

roughly constant, with a Thomson limited value of

$$\kappa_R \simeq 0.2(1 + X) \text{g cm}^{-2}, \quad (3)$$

where the hydrogen mass fraction in the disk is taken to be $X = 0.5$. Over the inner hundreds of kilometers of the disk, the optical depth is

$$\tau = \int \rho_0 \kappa_R dx \simeq 500 \gg 1, \quad (4)$$

where x is the space variable, and the integral is done over a length scale $L \sim 200$ km. This clearly indicates that the medium is optically thick to radiation. Finally, we consider the plasma to be a perfect gas with heat capacity at constant volume $c_v \simeq 4 \times 10^8$ erg g $^{-1}$ cm $^{-3}$.

Falize et al. (2011b) showed that the role of radiation in such flows can be characterized by two-dimensionless numbers. The first one, the Boltzmann number Bo, identifies the dominant energy transport mechanism and is defined as

$$\text{Bo} = \frac{\rho e(\rho, T) \nu}{\mathbb{F}_{\text{rad}}(T)}, \quad (5)$$

where e is the specific internal energy, ν the characteristic fluid velocity, and \mathbb{F}_{rad} the radiative flux. The Mihalas number, R, instead quantifies the radiative energy contribution with respect to internal energy density (Mihalas & Mihalas 1999), and is defined as

$$\text{R} = \frac{\rho e(\rho, T)}{\mathbb{E}_{\text{rad}}(T)}, \quad (6)$$

where \mathbb{E}_{rad} is the radiative energy density in the flow. In local thermodynamic equilibrium (LTE), radiation and matter temperatures are the same, T , and we take $\mathbb{E}_{\text{rad}} = a_R T^4$ with $a_R = 7.56 \times 10^{-15}$ erg cm $^{-3}$ K $^{-4}$ the radiative constant. In this case, the Mihalas number is, within a factor of order unity, the ratio between thermal pressure $P_{\text{th}} = \rho_0 e / (\gamma - 1)$ with $\gamma = 5/3$ the adiabatic index of the fluid, and radiative pressure $\mathbb{P}_{\text{rad}} = \mathbb{E}_{\text{rad}}/3$. For our simulation we have $\text{Bo} \sim 10^{-2}\text{--}10^{-4}$ and $\text{R} \sim 1\text{--}10^{-2}$. These values are characteristic of radiation-dominated regimes.

The simulations are carried out in a one-dimensional Cartesian geometry, with the RAMSES-RT code (Teyssier 2002; Rosdahl et al. 2013; Rosdahl & Teyssier 2015). RAMSES-RT solves the radiation hydrodynamic equations using a multi-group momentum-based resolution for the equations of radiative transfer (M1 method; González & Audit 2005). The simulations are run in the gray approximation, for a medium in LTE with radiation, allowing the photons to be scattered in an ionized medium. A blackbody radiation source is placed at the boundary $x = 0$ with a burst temperature $T_{\text{XRB}}(t)$ given by Equation (1). The computational domain, representing the inner region of the disk, is filled with a static, uniform density and temperature plasma that extends over 400 km. The grid has a uniform resolution $\Delta x \simeq 5 \times 10^3$ cm.

Typical results from the simulations are shown in Figure 1. The burst of radiation produces an RW that, in its initial propagation phase, leads at $t_1 = 0.05$ s to a temperature profile that is characteristic of supersonic Marshak waves. The leading edge of the RW is located at $x \sim 60$ km, indicating a propagation speed of the RW of ~ 1200 km s $^{-1}$, much larger than the characteristic sound (~ 300 km s $^{-1}$) and flow speeds (~ 100 km s $^{-1}$). Near the inner edge of the disk the density profile is only slightly altered by the radiative and thermal

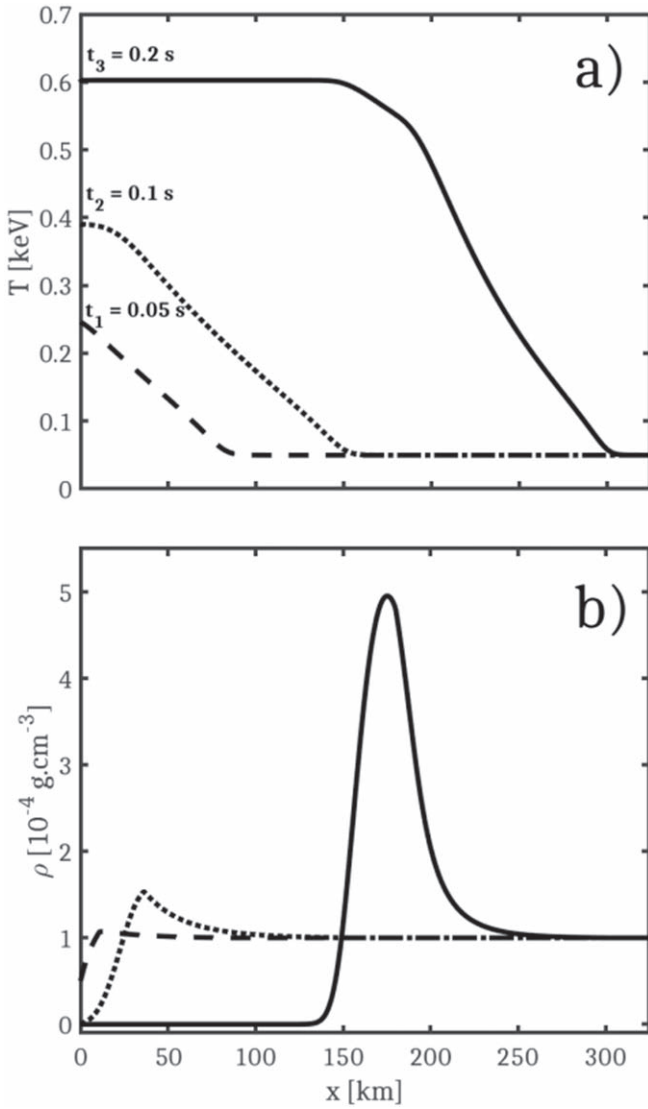


Figure 1. RAMSES-RT simulation of a radiation wave propagating through a simplified 1D accretion disk. The temperature (panel (a)) and density (panel (b)) profiles are shown at three different times ($t = 0.05$ s dashed lines; $t = 0.1$ s dotted lines, and $t = 0.2$ s straight lines). The transition from supersonic to subsonic regime occurs at $t \sim 0.2$ s and corresponds to an increase in density around $x \simeq 200$ km, hidden here by the compression of the medium but slightly visible on the temperature profile.

pressures. However, at $t_2 = 0.1$ s because of the fast rise time of the radiation burst, the increasing radiative pressure at the boundary begins to compress the internal regions of the disk, as shown in Figure 1(b). Indeed, over this time the Mihalas number taken at the inner boundary for a density ρ_0 decreases from $R \simeq 0.2$ at $t_1 = 0.05$ s to $R \simeq 0.05$ at $t_2 = 0.1$ s. At later times ($t_3 \simeq 0.2$ s) radiative pressure largely overcomes the thermal pressure of the plasma ($R \simeq 1.5 \times 10^{-2}$). The radiation acts as a piston that sweeps up the inner region of the disk leading to a constant temperature, optically thin low-density region extending up to $x \sim 150$ km. This drastic decrease of optical depth ($\tau \leq 1$) allows the XRBs photons to freely stream up to the optically thick high-density regions (~ 150 – 200 km). At this time, acoustic perturbations from the inner boundary, which is at temperature $T_{\text{XRB}} \sim 600$ eV, reach the radiative front leading to a phenomenon called hydrodynamic separation (Hammer & Rosen 2003; Garnier et al. 2006), which

corresponds to the transition to subsonic radiation waves. As the RW propagation becomes subsonic, the acoustic perturbations from the inner edge of the disk can accumulate at the radiative front leading to the creation of a shock at $x \simeq 200$ km. The transition from supersonic to subsonic regimes can be estimated theoretically by considering the time when the radiative front velocity equals the speed of sound taken at $x = 0$. This estimate gives $t \sim 0.2$ s, which is well recovered by the simulations. However, given the fast rise time of the XRB temperature the radiative front does not decelerate and keeps propagating ahead of the shock front. The latter effectively moves into an unshocked, but preheated medium, similar to the precursor of radiative shocks (Drake 2007).

The results presented are typical of strong radiation bursts irradiating their surrounding medium and show that RWs are likely to exist in such environments. However, the validity of numerical simulations in such radiation-dominated regimes needs to be assessed observationally or experimentally. In the following sections, we describe how RWs can be studied on a laboratory scale, and develop a theoretical framework to link experimental data to the simplified astrophysical system presented.

3. A New Approach Beyond Similarity for Laboratory Astrophysics: The Equivalence Symmetries

Nowadays, high-power laser and megajoule laser facilities such as NIF (Moses et al. 2009) and LMJ (Miquel & Prene 2019) allow producing and studying the evolution of radiation waves in the laboratory (Back et al. 2000a; Moore et al. 2015), including the transition from supersonic to subsonic propagation (Courtois et al. 2021). The characteristic parameters of laboratory experiments pursued on the Omega laser facility (Back et al. 2000a) and the National Ignition Facility (NIF; Moore et al. 2015) are given in Table 1. In particular, while the Boltzmann number $Bo \ll 1$, showing that the energy transport mechanism is purely radiative, these experiments have been carried out in regimes where the Mihalas number is $R > 1$, indicating that radiative energy density is much smaller than the thermal energy density. Under such conditions, the standard similarity approach (Falize et al. 2011b) does not allow for the scaling of the laboratory results to radiation-dominated astrophysical regimes, where $R \ll 1$.

To estimate the laser energy required to produce a radiation-dominated regime in the laboratory that could be scaled to astrophysics, we take the widely used experimental setup (Cohen et al. 2020) illustrated in Figure 2.

The experiment consists of irradiating the walls of a high-Z cavity (hohlraum), to convert a typical few nanoseconds pulse of laser energy into a burst of X-rays, which then irradiates a medium (usually a low-density foam). Using a typical model for the internal energy density of laboratory materials (Cohen et al. 2020), we find that reaching a Mihalas number of $R \simeq 0.2$ would require a typical radiation drive temperature of a few kiloelectronvolts. For characteristic experimental values (Back et al. 2000a) this corresponds to laser energy of approximately 10 MJ, which is well above the energy available in modern high-power laser facilities. Furthermore, besides the energy considerations, the equations of state and opacity laws should also be globally conserved (Falize et al. 2011a). In other words, to obtain global similarity experiments, the laboratory materials should still behave as a perfect gas in the Thomson opacity limit, which constitutes another stringent constraint that would be difficult to meet.

Table 1

Some Characteristics of Radiation Diffusion Waves in Accretion Disks Irradiated by X-Ray Bursts and Powerful Laser Facilities (Values from Characteristic Laser Experiments by Back et al. 2000b and Moore et al. 2015 Taken from Cohen et al. 2020)

| Environment | ρ_0 (g cm $^{-3}$) | T_{XRB} (eV) | L (cm) | τ | Bo | R |
|----------------------|--------------------------|-----------------------|-----------------|------------|--------------------|--------------------|
| Accretion disk | 10^{-4} | 400 | 2×10^7 | ~ 500 | 5×10^{-4} | 5×10^{-2} |
| Omega laser | 5×10^{-2} | 180 | 0.1 | ~ 5 | 10^{-2} | 35 |
| Megajoule facilities | 10^{-1} | 240 | 0.3 | ~ 10 | 5×10^{-3} | 20 |

Note. The Bo and R numbers are taken from the boundary at temperature T_{XRB} .

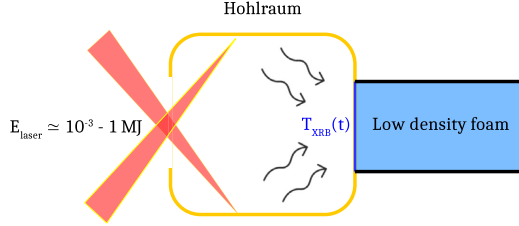


Figure 2. Schematic of a laser indirect drive experiment to produce RWs. The cavity (hohlraum) converts the nanosecond pulse of laser energy into X-rays, which then irradiate a low-density medium foam.

To move beyond similarity conditions, more general concepts are necessary. In this work, we seek to reproduce the physics of an astrophysical phenomenon under laboratory conditions without the need to conserve material properties or physical regimes. Such an approach belongs to the resemblance experiments category (Takabe 2001). As a first step in that direction, we focus on the supersonic regime of radiation waves, which occurs before any hydrodynamic motion alters the wave propagation ($t \lesssim 0.1$ s). This purely radiative transport phenomenon can be modeled by the balance between the variation of total energy density with time and the radiative flux carrying this energy through the system (Marshak 1958; Mihalas & Mihalas 1999), which is formally given by the transport equation:

$$\frac{\partial}{\partial t} [\rho e(\rho, T) + \mathbb{E}_{\text{rad}}(T)] + \vec{\nabla} \cdot [\vec{\mathbb{F}}_{\text{rad}}(T)] = 0. \quad (7)$$

For optically thick systems, we can use the diffusion approximation (Castor 2004), which gives us an analytical expression for the radiative flux:

$$\vec{\mathbb{F}}_{\text{rad}}(T) = -\frac{\lambda_R(\rho, T)c}{3} \vec{\nabla} (a_R T^4), \quad (8)$$

where $\lambda_R = 1/(\kappa_R \rho)$ is the Rosseland mean free path. Moreover, in the supersonic phase of interest, the density can be considered constant, so that we can now take the functions defining the plasma nature as $E(T) = \rho_0 e(T) + a_R T^4$ and $\lambda_R(T)$, dropping the density dependence.

We want to develop resemblance experiments, where the theoretical model defined by Equation (7) remains the same for both systems, while we allow for a modification of the nature of the medium, encoded in $E(T)$ and $\lambda_R(T)$, and of the radiation regime, characterized by Bo and R. We aim to do this by searching for equivalence symmetries of our systems. Following a method similar to that used by Ibragimov (2006) we looked for transformations of the variables x , t , T , $E(T)$, and $\lambda_R(T)$, appearing in the one-dimensional form of Equation (7). We found a six parameter Lie group of equivalence symmetries linking the set of astrophysical parameters, X_i , to the scaled laboratory parameters, \hat{X}_i . Of course, these transformations can

link any two systems, and take the general form

$$\hat{x} = \gamma_1 x + \gamma_4, \quad \hat{t} = \gamma_2 t + \gamma_5, \quad \hat{T} = \phi(T, \gamma_6), \quad (9)$$

$$\hat{\lambda}_R(\hat{T}) \phi^3 \frac{d\phi}{dT} = \gamma_3 \lambda_R(T) T^3, \quad \hat{E}(\hat{T}) = \frac{\gamma_2 \gamma_3}{\gamma_1^2} E(T), \quad (10)$$

where the γ_i are the real independent parameters of the transformations (Equations (9) and (10)), set by the choice of spatiotemporal scales and boundary conditions of the two systems. We see that this group of transformations contains two translations and scalings on x and t , whereas the transformation on T is completely arbitrary. Then, the presence of the functions $E(T)$ and $\lambda_R(T)$ in Equation (10) shows that it is now possible to modify their mathematical structure. In particular, there is proportionality between energy density distributions, while we observe a special form of transformation for $\hat{\lambda}_R(\hat{T})$. In other words, equivalence symmetries give us the freedom to modify the internal properties of the medium in which the RWs are propagating.

However, despite the apparent mathematical generality of these transformations, strong physical limitations appear when considering the real nature of astrophysical and laboratory plasmas. Indeed, assuming we know (E, λ_R) , we can see from Equations (9) and (10) that choosing a particular form for $\hat{\lambda}_R(\hat{T})$ sets constraints on the law $\phi(T)$ and consequently on the function $\hat{E}(\hat{T})$. Thus, the choice of laboratory materials ($\hat{E}, \hat{\lambda}_R$) will shape the mathematical form of the equivalence symmetries in our applications. Moreover, we find a new dimensionless number arising from the equivalence symmetries (Equations (9) and (10)), which is given by

$$\Pi = \frac{\rho_0 e(T)}{\mathbb{F}_{\text{rad}}(T)} \frac{x}{t} \left(1 + \frac{1}{R} \right), \quad (11)$$

where the first factor can be interpreted as a Boltzmann number and where R is given by Equation (6). The new dimensionless number Π is kept invariant by the transformations (Equations (9) and (10)), implying that the equivalence symmetries conserve some more general physical quantities between the systems than the similarity transformations.

In the following sections, we set the coefficient γ_4 and γ_5 equal to zero to exclude temporal and spatial shifting transformations. To gain further insights into the possibilities offered by the equivalence approach, we restrict the case of power-law functions for $\lambda_R(T) = \lambda_0 T^\alpha$ and $\hat{\lambda}_R(\hat{T}) = \hat{\lambda}_0 \hat{T}^{\hat{\alpha}}$, with λ_0 , $\hat{\lambda}_0$, α , and $\hat{\alpha}$ positive constants. This is a good approximation for typical laboratory materials in the appropriate temperature range. Such choice implicitly constrains the function ϕ describing the

temperature field transformation

$$\hat{T} = \phi(T, \gamma_6) = \left[\gamma_3 \gamma_6 \left(\frac{\lambda_0}{\hat{\lambda}_0} \right) T^{4+\alpha} \right]^{\frac{1}{4+\hat{\alpha}}}, \quad \gamma_6 = \frac{4 + \hat{\alpha}}{4 + \alpha} \quad (12)$$

and forces a particular distribution of energy density, that can be written only in terms of \hat{T} , giving

$$\hat{E}(\hat{T}) = \frac{\gamma_2 \gamma_3}{\gamma_1^2} E \left(\left[\frac{\hat{\lambda}_0}{\gamma_3 \gamma_6 \lambda_0} \right]^{\frac{1}{4+\alpha}} \hat{T}^{\gamma_6} \right). \quad (13)$$

We see that the function $\hat{E}(\hat{T})$ is completely described by Equation (13) as a function of only \hat{T} . This can lead to a very different energy density distribution for the transformed system compared to the initial one. This generalizes previous results (CEA, private communication) obtained by direct manipulation of Equation (7) in the limit of $\hat{R} \gg 1$. We stress that the possibility of linking different physical regimes goes well beyond the similarity approach whose major constraint remains in fact the conservation of physical regimes.

Now, we are still free to add constraints to the equivalent laboratory system. For example, if we set the internal energy density of both systems as power-law functions, we get $E(T) = e_0 T^\beta + a_R T^4$, and $\hat{E}(\hat{T}) = \hat{e}_0 \hat{T}^{\hat{\beta}} + a_R \hat{T}^4$, choosing e_0 , \hat{e}_0 , β , and $\hat{\beta}$ as positive constants. By setting a particular form for $\hat{E}(\hat{T})$, we can recover previous results from the literature. Here, we lost the freedom of choosing the exponents $\hat{\alpha}$ and $\hat{\beta}$, giving

$$\hat{\alpha} = \alpha, \quad \hat{\beta} = \beta. \quad (14)$$

In this case, the equivalence transformations (Equations (9) and (10)) degenerate into the scaling laws for radiation-dominated systems described by Falize et al. (2011b), in the supersonic approximation. Moreover, in the limit of strong Mihalas numbers ($R \gg 1, \hat{R} \gg 1$), we can neglect the radiative energy density contributions, which gives us $E(T) = e_0 T^\beta$ and $\hat{E}(\hat{T}) = \hat{e}_0 \hat{T}^{\hat{\beta}}$. Still considering power laws for λ_R and $\hat{\lambda}_R$, this immediately leads to drastic constraints on the α and β exponents, along with an entire set of transformations given by

$$\frac{\hat{x}}{x} = \gamma_1, \quad \frac{\hat{t}}{t} = \gamma_2, \quad \frac{\hat{\lambda}_0}{\lambda_0} = a_\lambda, \quad \frac{4 + \hat{\alpha}}{4 + \alpha} = \gamma_6, \quad (15)$$

$$\frac{\hat{e}_0}{e_0} = \frac{\gamma_2 \gamma_3}{\gamma_1^2} \left(\frac{a_\lambda}{\gamma_3 \gamma_6} \right)^{\frac{\beta}{4+\alpha}}, \quad \frac{\hat{\beta}}{\beta} = \gamma_6, \quad (16)$$

$$\hat{T} = \left[\frac{\gamma_3 \gamma_6}{a_\lambda} \right]^{\frac{1}{4+\alpha}} T^{\frac{1}{\gamma_6}}, \quad (17)$$

where a_λ is a free constant parameter. This can be seen as generalized scaling laws that lead to the conservation of another parameter:

$$\frac{\hat{\beta}}{4 + \hat{\alpha}} = \frac{\beta}{4 + \alpha}. \quad (18)$$

This particular term is the ϵ parameter of Hammer & Rosen (2003), which characterizes the steepness of the radiative front and arises naturally from these symmetry considerations. Moreover, by choosing a homothetic relation between \hat{T} and T

($\gamma_6 = 1$), we find that the constraint (Equation (18)) splits into Equation (14). This leads us to retrieve the scaling laws for weakly radiative regimes (Falize et al. 2011b). Thus, homothetic scaling laws appear as the natural limit of the equivalence transformations found here.

4. Numerical Simulations: From Accretion Disks to the Laboratory

We are now going to use the equivalence symmetries given by Equations (9) and (10) to design an experiment with $\hat{R} \gg 1$ able to mimic the RW simulated for the astrophysical conditions with $\hat{R} \leq 1$ of Section 2. The experimental setup is based on the one illustrated in Figure 2.

The astrophysical system is that described in Section 2, and for the application here it is defined in terms of its total energy $E(T) = \rho_0 c_v T + a_R T^4$, and Thomson scattering opacity $\lambda_R(T) = \lambda_0$. These choices constrain the laboratory system, where we can now only set either the form of the energy $\hat{E}(\hat{T})$ or the opacity law represented by the function $\hat{\lambda}_R(\hat{T})$. Setting one of them automatically imposes the other through the equivalence symmetries (Equations (9) and (10)). While either choice is theoretically possible, in practice the limitations on the available opacity laws for laboratory materials means that the latter has to be set. Consistent with characteristic expression for laboratory materials (Cohen et al. 2020), we take $\hat{\lambda}_R(\hat{T}) = \hat{\lambda}_0 \hat{T}^{\hat{\alpha}}$. The choice $\hat{\alpha} = 2.22$ fixes the value $\gamma_6 \simeq 1.55$, and the mathematical form of the energy $\hat{E}(\hat{T})$ is then given by Equation (13). We are now left with the choice of the three scaling parameters γ_1 , γ_2 , and γ_3 that appear in the equivalence transformations (Equations (9) and (10)), and which are set by establishing spatial and temporal scales for the laboratory system, along with specific boundary conditions. These are discussed next.

The spatial and temporal scales of the astrophysical supersonic RW are taken respectively at 2×10^7 cm and 10^{-1} s, whereas those of the laboratory system will typically be of the order of 0.4 cm and 10^{-8} s. From the equivalence transformations (Equations (9) and (10)), those choices set $\gamma_1 = 2 \times 10^{-8}$ and $\gamma_2 = 10^{-7}$. The use of equivalence symmetries also affects the boundary condition $T_{\text{XRB}}(t)$, implying that the shape of the burst created in the laboratory $\hat{T}_{\text{XRB}}(\hat{t})$ must be equivalent to the astrophysical one, a constraint most laser facilities could achieve. The maximum temperature reached by the astrophysical XRB during the supersonic regime is $T_R = 400$ eV, and we chose to take an equivalent laboratory temperature of $\hat{T}_R = 250$ eV commonly reached on megajoule facilities, setting $\gamma_3 = 6.67 \times 10^{-8}$. We note that the choice of initial density is completely free of constraints at this point, and we take $\hat{\rho}_0 = 0.04$ g cm $^{-3}$ as a typical value for foam targets.

The procedure outlined sets the remaining laboratory parameters, namely, the internal energy density given by Equation (13) and the initial temperature of the foam \hat{T}_0 given by Equation (12). For the latter, the equivalence transformations impose an initial temperature for the foam $\hat{T}_0 \sim 60$ eV. However, for the experimental setup under consideration here, having an initially hot medium is very difficult in practice. Therefore, for the experimental design and the simulations presented in the following, we considered lower disk temperatures ($T_0 = 1$ eV). As was pointed out in Section 2, the temperature of the disk does not qualitatively alter the RW regime of propagation. To be consistent with the previous

Table 2

Values of the Characteristic Parameters of the Two Equivalent Systems, Along the Value of the Equivalence Parameters, Where γ_1 , γ_2 , and γ_3 Are Given in Equations (9) and (10) and γ_6 is Taken from Equation (15)

| | Accretion Disk | Laboratory |
|----------------------------------|-----------------------|------------------------|
| ρ_0 [g cm $^{-3}$] | 10^{-4} | 4×10^{-2} |
| T_{XRB} [eV] | 400 | 250 |
| t [s] | 10^{-1} | 10^{-8} |
| L [cm] | 2×10^7 | 0.4 |
| α | 0 | 2.22 |
| λ_0 [cm K $^{-\alpha}$] | 3.33×10^4 | 1.02×10^{-16} |
| ρe [erg cm $^{-3}$] | $\rho c_v T$ | Equation (13) |
| R | 5×10^{-2} | 120 |
| Equivalence parameters | | |
| γ_1 | 2×10^{-8} | |
| γ_2 | 10^{-7} | |
| γ_3 | 6.67×10^{-8} | |
| γ_4 | 0 | |
| γ_5 | 0 | |
| γ_6 | 1.55 | |

analysis, for the astrophysical case we keep the Thomson opacity hypothesis even for these low disk temperatures. However, we stress that the equivalence transformations are not restricted to that particular choice for the opacity (or equations of state). This further highlights the remarkable adaptability of the new equivalence approach, which is only used here in a very particular case in terms of opacity laws and equations of state. A summary of the physical and equivalence parameters for our example is given in Table 2.

One-dimensional numerical simulations of the experiments are performed with the CEA laser radiation hydrodynamics arbitrary Lagrangian-Eulerian code FCI2 (Schurtz et al. 2000). We used the multi-group diffusion model (100 groups) and tabulated the equation of state and mean free path, created with respect to the equivalence constraints (Equations (12) and (13)). A comparison between the simulations in the laboratory and astrophysical systems is shown in Figure 3.

At early times, we see that the agreement between the two simulations is very good, with the largest deviation in the transformed temperature profiles being $< 1\%$. Similarly, the radiative front positions ($x_f(t)$, $\hat{x}_f(\hat{t})$) correspond exactly after transformation, with a deviation $< 1\%$. At later times, $t \sim 0.05$ s or equivalently $\hat{t} \sim 5$ ns, the radiation-dominated front starts to accelerate, showing an increasing deviation of $\simeq 3\%$ for temperature and $\simeq 1\%$ for the position of the front. Finally, at $t \sim 0.1$ s, or equivalently $\hat{t} \sim 10$ ns, we see a clear deviation from equivalence ($\simeq 12\%$ for temperatures and $\simeq 3\%$ for the front position). At this time the disk motion and the beginning of hydrodynamic separation deeply modify the structure of the astrophysical radiation wave. Thus, we find that our results hold until we reach a temperature $T_{\text{XRB}} \simeq 300$ eV, or equivalently $\hat{T}_{\text{XRB}} \simeq 210$ eV, which is a value megajoule laser facilities could easily reach (Moore et al. 2015). More generally, any application of the equivalence transformations given by Equations (9) and (10) is limited by the fact that both systems must be described by the theoretical model given by Equations (7) and (8). One of the principal limitations for the application of the equivalence transformations to astrophysical and laboratory RWs thus appears to be the hydrodynamic motion of the plasma, which can be triggered at the transition to the subsonic regime. We note that this transition happens after a certain hydrodynamic separation time

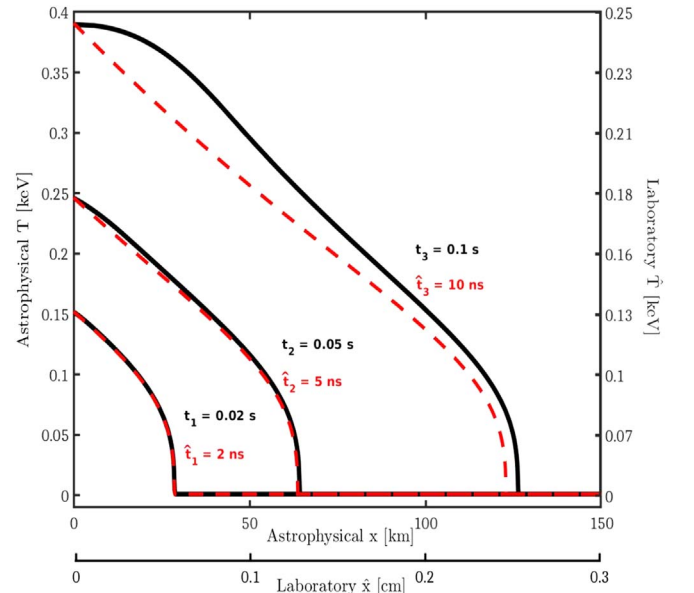


Figure 3. Comparison of a full radiation hydrodynamic simulation of the astrophysical system (black solid lines) from RAMSES-RT to the equivalent laboratory system after transformation (red dashed lines) from FCI2, in terms of spatial temperature profiles.

that can be theoretically assessed only in some simplified cases (Garnier et al. 2006).

To conclude, even if this example only constitutes an arbitrary theoretical choice of laboratory material (\hat{E} , $\hat{\lambda}_R$), and physical regime (\hat{B}_0 , \hat{R}), it allows us to prove how much this kind of analysis can be useful to find new ways of confronting numerical results in unknown regimes to potential experiments. The complete design of an equivalent experimental setup will be the subject of a future dedicated paper.

5. Discussion

In this paper, we aim to provide a first insight into how laboratory astrophysics could benefit from symmetry concepts. To this end, we created a simplified XRB-disk interaction model to show the propagation of RWs on astrophysical scales. In order to find resemblance transformations for those systems, we developed for the first time equivalence symmetries of RWs. We found that these powerful tools generalize the global invariance concept and its resultant scaling laws, thus overcoming the similarity constraints. These results were confirmed by numerical simulations using the RAMSES-RT and FCI2 codes.

The major contribution of the equivalence approach resides in the possibility of modeling the transformations using physical arguments based on theoretical material properties. Indeed, much effort has already been done in finding generalized similarity transformations for diffusion-transport equations (Munier et al. 1981; Burgan et al. 1984), but leading to mathematical constraints on plasma nature functions that were nonphysical. Moreover, in any radiation hydrodynamic experiments, the correct characterization of material properties, here in terms of the equation of state and opacity law, constitutes a basic assumption. In this paper, these have been assessed theoretically in order to get a first insight into how the equivalence concept works. It is now known that uncertainties in materials' equation of state and opacity law can strongly

affect laboratory experiments (Fryer et al. 2016; Heeter et al. 2017). However, Equations (9–10) show that proper spatio-temporal scaling could be able to account for material properties' experimental deviations. This particularly stresses the appeal of equivalence methods for such laboratory experiments. Determining the effects of uncertainties on a material's internal properties onto potential equivalent experiments will be discussed in a future paper dedicated to the experimental section of this work.

New possibilities now appear in order to study theoretically the interaction of a Type I XRB with its surrounding accretion disk in a more global fashion with two kinds of experiments. The first one should be based on the supersonic phase of the radiation wave described in this paper. Then, a second experiment should focus on the transonic and subsonic phases, as was recently done by Courtois et al. (2021). In this case, the application of the equivalence symmetries given by Equations (9) and (10) leads to the addition of extra terms in the energy conservation equation, which depend directly on the density derivatives and cannot be neglected anymore. In order to study subsonic heat waves, an extended set of symmetries would have to be considered (Coggeshall & Axford 1986). In particular, in these regimes ($\dot{R} > 1$), radiation hydrodynamics scaling laws (Falize et al. 2011b) could theoretically be used. This could lead to new kinds of experiments based on a generalized approach considering both similarity and resemblance transformations applied to different physical regimes.

Furthermore, the equivalence concept only represents the first step toward more generalized approaches for laboratory astrophysics. One promising avenue is to use mapping techniques (Bluman et al. 2010) to find more complex analogy transformations. Examples include the physics of Hawking radiation emanating from an analog black hole in atomic Bose–Einstein condensates (Unruh 1981; Steinhauer 2016), or optical-mechanical analogy to study celestial mechanics in meta-materials (Genov et al. 2009). These concepts could lead to the development of a new class of transformations able to capture transitory phenomena such as hydrodynamic separation. These ideas constitute the starting point of the MaTaLE (Mapping Theory and Laser Experiments) project, an experimental platform dedicated to this brand new laboratory of astrophysics.

Finally, the constraint imposed by the equivalence symmetries can lead to particular forms of equations of state and photon mean free paths that may not be yet representative of what we know about any laboratory media. This could open the way to technological developments in the area of meta-materials (Leonhardt 2006), allowing for modification of the internal properties of laboratory media to perfectly match the equivalent system. This offers new perspectives to study a multitude of previously unreachable astrophysical systems in megajoule facilities in the next decades.

We would like to thank Joki Rosdahl for his help in the adaptation of the RAMSES-RT code for this work.

ORCID iDs

V. Tranchant  <https://orcid.org/0000-0002-7565-0804>

References

Albertazzi, B., Ciardi, A., Nakatsutsumi, M., et al. 2014, *Sci*, **346**, 325
 Albertazzi, B., Mabey, P., Michel, T., et al. 2020, *PhPI*, **27**, 022111
 Back, C. A., Bauer, J. D., Hammer, J. H., et al. 2000b, *PhPI*, **7**, 2126

Back, C. A., Bauer, J. D., Landen, O. L., et al. 2000a, *PhRvL*, **84**, 274
 Ballantyne, D. R., & Everett, J. E. 2005, *ApJ*, **626**, 364
 Bluman, G. W., Cheviakov, A. F., & Anco, S. C. 2010, *Applications of Symmetry Methods to Partial Differential Equations* (Berlin: Springer), 121
 Burgan, J. R., Munier, A., Feix, M. R., & Fijalkow, E. 1984, *SJAM*, **44**, 11
 Burns, R. A., Sugiyama, K., Hirota, T., et al. 2020, *NatAs*, **4**, 506
 Castor, J. I. 2004, *Radiation Hydrodynamics* (Cambridge: Cambridge Univ. Press)
 Ciardi, A., Lebedev, S. V., Frank, A., et al. 2007, *PhPI*, **14**, 056501
 Ciardi, A., Lebedev, S. V., Frank, A., et al. 2009, *ApJL*, **691**, L147
 Ciardi, A., Vinci, T., Fuchs, J., et al. 2013, *PhRvL*, **110**, 025002
 Coggeshall, S. V., & Axford, R. A. 1986, *PhFI*, **29**, 2398
 Cohen, A. P., Malamud, G., & Heizler, S. I. 2020, *PhRvR*, **2**, 023007
 Courtois, C., Robert, C., Bretheau, D., et al. 2021, *PhPI*, **28**, 073301
 Cross, J., Gregori, G., Foster, J., et al. 2016, *NatCo*, **7**, 1
 Dale, J. E., Ngoumou, J., Ercolano, B., & Bonnell, I. A. 2014, *MNRAS*, **442**, 694
 Drake, R. P. 2007, *PhPI*, **14**, 043301
 Falize, E., Dizière, A., & Loupiau, B. 2011a, *Ap&SS*, **336**, 201
 Falize, É., Michaut, C., & Bouquet, S. 2011b, *ApJ*, **730**, 96
 Fragile, P. C., Ballantyne, D. R., & Blankenship, A. 2020, *NatAs*, **4**, 541
 Fragile, P. C., Ballantyne, D. R., Maccarone, T. J., & Witry, J. W. L. 2018, *ApJL*, **867**, L28
 Fryer, C., Dodd, E., Even, W., et al. 2016, *HEDP*, **18**, 45
 Galloway, D. K., & Keek, L. 2021, *Timing Neutron Stars: Pulsations, Oscillations and Explosions* (Berlin: Springer), 209
 Garnier, J., Malinić, G., Saillard, Y., & Cherfils-Clérouin, C. 2006, *PhPI*, **13**, 092703
 Genov, D. A., Zhang, S., & Zhang, X. 2009, *NatPh*, **5**, 687
 González, M., & Audit, E. 2005, *Ap&SS*, **298**, 357
 Hammer, J. H., & Rosen, M. D. 2003, *PhPI*, **10**, 1829
 Heeter, R., Bailey, J., Craxton, R., et al. 2017, *JPIPh*, **83**, 595830103
 Ibragimov, N. H. 2006, *Selected works. Volumes 1-4* (Blekinge: ALGA publications, BTH)
 Keek, L., Arzoumanian, Z., Bult, P., et al. 2018, *ApJL*, **855**, L4
 Krauland, C., Drake, R., Kuranz, C., et al. 2012, *ApJL*, **762**, L2
 Krauland, C., Drake, R., Kuranz, C., et al. 2013, *PhPI*, **20**, 056502
 Kuranz, C. C., Park, H. S., Huntington, C. M., et al. 2018, *NatCo*, **9**, 1564
 Lebedev, S. V., Ciardi, A., Ampleford, D. J., et al. 2005, *MNRAS*, **361**, 97
 Leonhardt, U. 2006, *Sci*, **312**, 1777
 Lewin, W. H. G., van Paradijs, J., & Taam, R. E. 1993, *SSRv*, **62**, 223
 Mabey, P., Albertazzi, B., Falize, E., et al. 2019, *NatSR*, **9**, 8157
 Marshak, R. E. 1958, *PhFI*, **1**, 24
 Mihalas, D., & Mihalas, B. W. 1999, *Foundations of Radiation Hydrodynamics* (Mineola, NY: Dover)
 Miquel, J.-L., & Prene, E. 2019, *NucFu*, **59**, 032005
 Moore, A. S., Guymer, T. M., Morton, J., et al. 2015, *JQRST*, **159**, 19
 Morris, M. A., Weidenschilling, S. J., & Desch, S. J. 2016, *M&PS*, **51**, 870
 Moses, E. I., Boyd, R. N., Remington, B. A., Keane, C. J., & Al-Ayat, R. 2009, *PhPI*, **16**, 041006
 Munier, A., Burgan, J., Gutierrez, J., Fijalkow, E., & Feix, M. 1981, *SJAM*, **40**, 191
 Norris, J. P., Bonnell, J. T., Kazanas, D., et al. 2005, *ApJ*, **627**, 324
 Olver, P. J. 1986, *Applications of Lie Groups to Differential Equations*, Vol. 107 (New York, NY: Springer Science & Business Media)
 Ovsiannikov, L. V. 1982, *Group Analysis of Differential Equations* (New York: Academic)
 Falize, É., Ravasio, A., Loupiau, B., et al. 2012, *HEDP*, **8**, 1
 Revet, G., Chen, S. N., Bonito, R., et al. 2017, *SciA*, **3**, e1700982
 Revet, G., Khair, B., Filippov, E., et al. 2021, *NatCo*, **12**, 762
 Rigon, G., Casner, A., Albertazzi, B., et al. 2019, *PhRvE*, **100**, 021201
 Rosdahl, J., Blaizot, J., Aubert, D., Stranex, T., & Teyssier, R. 2013, *MNRAS*, **436**, 2188
 Rosdahl, J., & Teyssier, R. 2015, *MNRAS*, **449**, 4380
 Ryutov, D., Drake, R. P., Kane, J., et al. 1999, *ApJ*, **518**, 821
 Schurtz, G. P., Nicolai, P. D., & Busquet, M. 2000, *PhPI*, **7**, 4238
 Steinhauer, J. 2016, *NatPh*, **12**, 959
 Takabe, H. 2001, *PThPS*, **143**, 202
 Teyssier, R. 2002, *A&A*, **385**, 337
 Unruh, W. G. 1981, *PhRvL*, **46**, 1351
 Valenzuela-Villaseca, V., Suttle, L., Suzuki-Vidal, F., et al. 2022, arXiv:2201.10339
 Van Box Som, L., Falize, E., Koenig, M., et al. 2018, *High Power Laser Sci. Eng.*, **6**, E35
 Walch, S. K., Whitworth, A. P., Bisbas, T., Wünsch, R., & Hubber, D. 2012, *MNRAS*, **427**, 625